



NativeTok: Native Visual Tokenization for Improved Image Generation

Bin Wu Mengqi Huang* Weinan Jia Zhendong Mao

{lilimotion,jiawn}@mail.ustc.edu.cn, {zdmq,huangmq}@ustc.edu.cn

University of Science and Technology of China

Abstract

VQ-based image generation typically follows a two-stage pipeline: a tokenizer encodes images into discrete tokens, and a generative model learns their dependencies for reconstruction. However, improved tokenization in the first stage does not necessarily enhance the second-stage generation, as existing methods fail to constrain token dependencies. This mismatch forces the generative model to learn from unordered distributions, leading to bias and weak coherence. To address this, we propose **native visual tokenization**, which enforces causal dependencies during tokenization. Building on this idea, we introduce **NativeTok**, a framework that achieves efficient reconstruction while embedding relational constraints within token sequences. NativeTok consists of: (1) a **Meta Image Transformer (MIT)** for latent image modeling, and (2) a **Mixture of Causal Expert Transformer (MoCET)**, where each lightweight expert block generates a single token conditioned on prior tokens and latent features. We further design a Hierarchical Native Training strategy that updates only new expert blocks, ensuring training efficiency. Extensive experiments demonstrate the effectiveness of NativeTok.

Project Page: <https://github.com/wangbei1/Nativetok>

1 Introduction

Over the past few years, the vision community has witnessed remarkable progress in deep generative models, such as diffusion models[14, 18, 25, 26, 28] and autoregressive models[5, 10, 12, 16, 23, 30, 32, 36], elevating image generation quality to unprecedented levels. Inspired by the success of large language models (LLMs), large visual models have recently attracted increasing research interest, primarily due to their compatibility with established innovations from LLMs (*e.g.*, scaling laws) and their potential to unify language and vision towards general artificial intelligence (AGI). Different from the natural tokenization for language such as BPE (Byte Pair Encoding)[3, 29], the visual tokenization, *i.e.*, converting images into discrete tokens analogous to those used in language models, remains a longstanding challenge for VQ-Based large visual models.

Most modern large visual models follow a two-stage paradigm, *i.e.*, (1) the first *tokenization stage* learns an image tokenizer by reconstructing images, converting high-dimensional pixels into compressed discrete visual tokens, and (2) the second *generation stage* trains a generative model to model the token distribution via next-token prediction.

Recent works have focused on designing improved image tokenizers with higher compression ratios to accelerate

* Corresponding author.

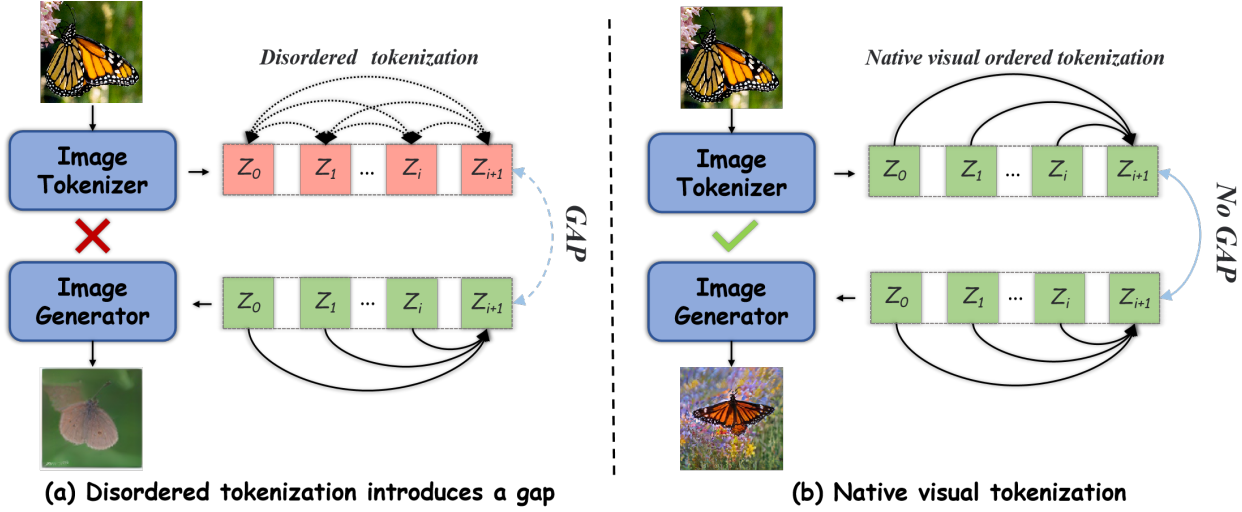


Figure 1 Illustration of our motivation. (a) Existing *disordered tokenization* overlooks the essential requirement of relational modeling in the generation stage, as it fails to introduce any token dependency constraints during tokenization, resulting in a gap between the two stages of image generation. (b) Our approach proposes **native visual tokenization**, which considers not only reconstruction quality but also imposes relational constraints during tokenization, thereby coupling the two stages of image generation.

generation process, or higher reconstruction quality to enhance generation quality. For example, DQVAE [19] introduces a more compact tokenizer by dynamically allocating varying numbers of tokens to image regions based on their information density. VAR [31] proposes a multi-scale tokenizer combined with a coarse-to-fine "next-scale prediction" generation strategy. TiTok [37] significantly accelerates generation by compressing images into shorter one-dimensional serialized representations. In summary, existing methods primarily focus on first independently designing a better tokenizer, and then training a generative model to capture the distribution of the resulting visual tokens.

However, we argue that existing methods overlook the intrinsic dependency between the tokenization and generation stages, optimizing each stage with separate objectives. This leads to a fundamental misalignment between the disordered tokenization outputs and the structured dependency modeling required during generation. Specifically, as illustrated in Fig.1(a), the first stage typically relies on reconstruction loss for supervision during tokenization, without imposing constraints on the intrinsic relationships among tokens, while the second stage essentially models the intrinsic distributional relationships among the tokens learned in the first stage. This misalignment prompts a critical inquiry: **How can a generative model accurately learn visual token distributions if the tokens themselves are inherently disordered in nature?**

As a result, the generation stage can only learn a biased and incomplete distribution from these disordered visual tokens, leading to sub-optimal generative performance. Moreover, a persistent gap exists in current two-stage generation paradigm, *i.e.*, better tokenization performance in the first stage does not necessarily result in improved generation in the second stage, as it may lead to more complex token interrelationships that further violates the autoregressive principle.

To address the above challenge, we introduce the concept of *native visual tokenization*, which tokenizes images in a native visual order that inherently aligns with the subsequent generation process, leading to more effective and accurate visual token modeling, as illustrated in Fig.1(b). **We argue that visual information in an image also follows a global causal order. Analogous to human perception, when observing an image, we tend to first recognize its primary structural components, followed by finer details such as textures.** This observation suggests that the process of visual understanding is inherently autoregressive in nature. Built upon this concept, we propose **NativeTok**, a novel visual tokenization framework that disentangles *visual context modeling* from *visual dependency modeling*, thereby enabling the joint optimization of image reconstruction quality and token ordering without conflict. As a result, NativeTok is capable of producing a native visually ordered

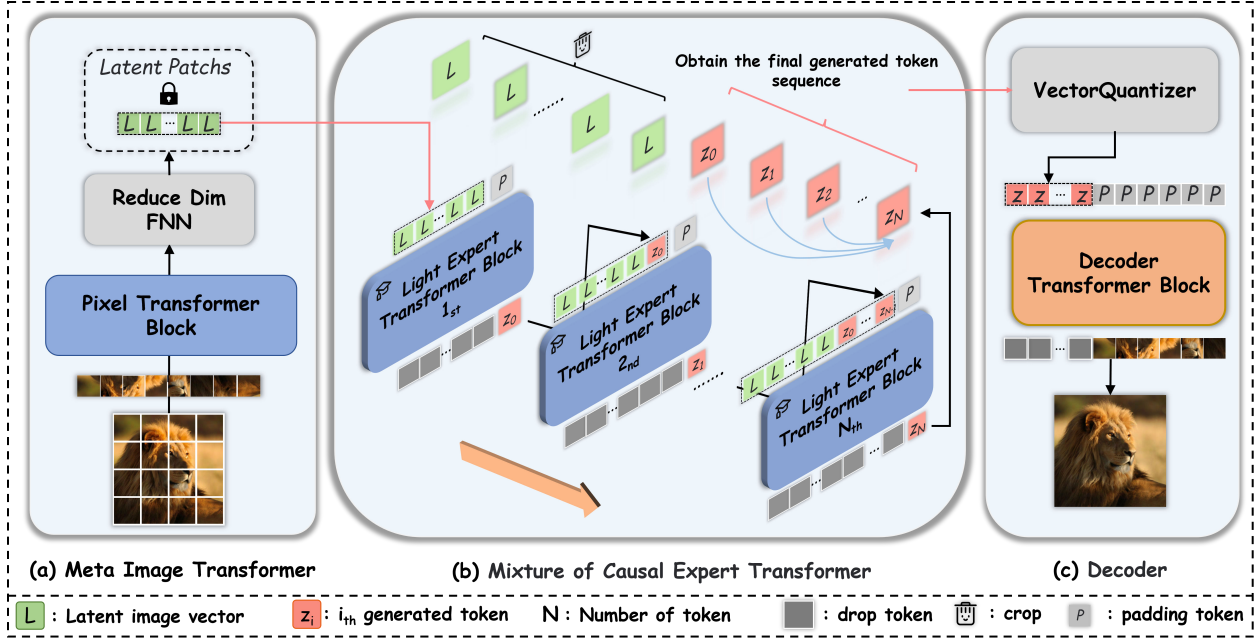


Figure 2 The overview of our NativeTok framework. (a) In Meta Image Transformer (MIT), the image information is initially modeled by a Pixel Transformer, then compresses the image into the latent space. During the subsequent generation process, the latent space information of the image remains locked. (b) During the token sequence generation process, we define Mixture of Causal Expert Transformer (MoCET). The i^{th} expert transformer block is responsible for generating the i^{th} token. In each generation step, we concatenate the locked latent space image information, all previously generated tokens, and the current mask token, and feed them into the corresponding expert transformer. Once a token is generated, it remains fixed. (c) Once all tokens are generated, they are fed into the decoder to reconstruct the image.

token sequence directly during the tokenization stage. Specifically, NativeTok comprises three components: (1) the *Meta Image Transformer (MIT)*, which models image patch features with high-dimension for effective visual context modeling, followed by a dimension switcher that compresses the context output for subsequent efficient visual dependency modeling. (2) The *Mixture of Causal Expert Transformer (MoCET)* features a novel ensemble of lightweight expert transformer blocks, each tailored to a specific token position. This position-specific specialization allows MoCET to model causal dependencies with greater precision, yielding an ordered token representation. (3) Finally, the ordered token representation is quantized into discrete tokens and subsequently decoded by a transformer-based decoder. Moreover, we further propose a novel *Hierarchical Native Training* strategy to efficiently train NativeTok across varying tokenization lengths. NativeTok not only accomplishes the reconstruction task of the first stage but also explicitly constrains the intrinsic relationships within the token sequence, making it easier for the second-stage generation process to capture and model these dependencies, thereby achieving a close integration between the two stages.

2 Related Work

2.1 Image Tokenization

Image Tokenization is a fundamental and crucial step in image generation. Image tokenization involves using autoencoders to compress images from high-dimensional, high-resolution space into a low-dimensional, low-resolution latent space, and then using a decoder to reconstruct the image from this latent space. CNN-based autoencoder tokenizers, such as VQ-VAEs [27, 32], encode images to a discrete representation, forming a codebook of image information. DQ-VAE [19] focuses on the information density of different image regions and encodes images using information-density-based variable-length coding. Transformer-based autoencoder tokenizers, such as ViT-VQGAN [35] and Efficient-VQGAN [4], also achieve excellent reconstruction results

through the use of transformers. Titok [37] and MAETok[7] achieves excellent reconstruction results by compressing images into one-dimensional sequences with a high compression ratio. Many works further explore improvements in the vector quantization step, such as SoftVQ[6], MoVQ[38], and RQ-VAE[22], while FSQ [24] propose LFQ methods. In recent work, FlexTok [1] incorporates characteristics of continuous VAEs, utilizing flexible-length 1D encodings to enable a visually ordered reconstruction process, while GigaTok [34] also achieve wonderful generation results. However, these works completely neglects the dependency relationships among tokens that need to be modeled in the second stage, resulting in a fundamental discrepancy between the token dependencies established in the first stage and the image modeling approach in the second stage and do not treat the two stages as a unified process. Therefore, we propose NativeTok, which introduces strong constraints when modeling token dependencies to capture more accurate intrinsic relationships. This enables the generator to more easily learn such associations during the generation process, thereby achieving a true integration of the tokenization and generation stages.

2.2 Image Generation

Image Generation typically learns and generates images from the image latent space generated in the image tokenization stage, which enhances generation efficiency. Existing generation methods primarily include three paradigms: GANs[13, 15, 20, 21], diffusion models[14, 18, 25, 26, 28], and autoregressive models[5, 10, 12, 16, 23, 30, 32, 36]. These methods predict the next token or group of tokens, based on conditions and previously generated tokens, until the entire token sequence is generated. However, previous image tokenization approaches fail to consider the inherent requirement of the second-stage generator to model the internal dependencies among tokens. As a result, the generated unordered sequence can only lead to a biased and inherently inaccurate model.

3 Methodology

3.1 NativeTok framework

To achieve the goal of *native visual tokenization* and ensure tight integration between the tokenization and generation stages, we design the **NativeTok** framework, as illustrated in Fig. 2. As previously discussed, our aim is to model the ordered relationships among tokens during the tokenization stage. This requires the first-stage tokenization process to ultimately produce an ordered, causally token sequence that aligns with the native visual order:

$$z_i = \text{Encoder}(\mathbf{X}, z_0, z_1, \dots, z_{i-1}). \quad (1)$$

The modeling of token z_i depends only on the previous tokens z_0 to z_{i-1} and the image information \mathbf{X} , and is independent of any subsequent $z_{j(j>i)}$.

To achieve such a generation process, a naive approach is to apply a causal mask [33]. However, we find that this method is ineffective in practice, as the transformer must simultaneously perform image self-modeling and token generation, making it difficult to generate tokens sequentially. Moreover, its performance heavily depends on the capacity of the original model and does not yield substantial improvements, as confirmed by the experimental results presented in the subsequent ablation studies.

Therefore, we propose a novel framework that adopts a divide-and-conquer design. It decouples complex context modeling of image content from the dependency modeling among image tokens. In the image context modeling stage, we employ bidirectional attention to capture global representations of the image. In the token dependency modeling stage, we introduce native visual constraints for token-level dependency modeling, while still allowing each token to adaptively attend to the full image context.

Specifically, the NativeTok framework consists of the following two components:

Meta Image Transformer (MIT): Instead of directly using the original image embedding for token modeling, we first model the input image \mathbf{X} through the Meta Image Transformer *MIT*, which consists of a series of transformers, followed by a fully connected network (FNN) acting as a dimension switcher to reduce

dimensionality, ultimately obtaining $\mathbf{X}_{\text{latent}}$, where $\mathbf{X}_{\text{latent}}$ represents the rich contextual information of the image in the latent space.

$$\mathbf{X}_{\text{latent}} = \text{FNN}(\text{MIT}(\mathbf{X})). \quad (2)$$

Mixture of Causal Expert Transformer (MoCET): Each token used for representation is modeled by a separate expert transformer. Specifically, our generation process is as follows: (1) Lock $\mathbf{X}_{\text{Latent}}$, keeping it unchanged during the generation process to ensure that each subsequent token generation focuses on the same image information. (2) we define an ordered lightweight expert transformer sequence

$$\mathbb{T} = \{\mathbb{T}_0, \mathbb{T}_1, \dots, \mathbb{T}_L\}, \quad (3)$$

of the same length L as the token sequence. The i^{th} expert transformer block of \mathbb{T} is solely responsible for generating the i^{th} token. (3) In the generation step of each token, we concatenate the locked latent space image information, all previously generated tokens, and the current padding token, and feed them into the corresponding transformer. We retain only a single vector from the original padding token positions as the currently generated token. For example, in the generation process of the i^{th} token:

$$\mathbf{z}_i = \mathbb{T}_i(\mathbf{X}_{\text{latent}}, \mathbf{z}_0, \mathbf{z}_1, \dots, \mathbf{z}_{i-1}, \mathbf{z}_{\text{padding}}), \quad (4)$$

where \mathbb{T}_i denotes the expert transformer block responsible for modeling the i^{th} token in the Mixture of Causal Experts \mathbb{T} . The tokens \mathbf{z}_j ($j < i$) represent those that have already been generated, and \mathbf{z}_i refers to the current token modeled at the position of $\mathbf{z}_{\text{padding}}$. Once \mathbf{z}_i is generated, it is fixed and incorporated into the modeling of subsequent tokens, and the process continues until the entire token sequence is produced.

The divide-and-conquer design of NativeTok enables the modeling of visual token dependencies while allowing each image token to adaptively select from the global image context. This strategy aligns well with the previously discussed human perception-inspired modeling paradigm, which progresses from global structures to finer details.

Image generation: To comprehensively evaluate the impact of explicitly introducing constraints during the tokenization stage, we conduct experiments using both autoregressive (AR) and MaskGIT-style generation frameworks. For the AR setting, we adopt LlamaGen [11] as the generator, while for the MaskGIT setting, we follow recent work [2, 5].

3.2 Training: Hierarchical Native Training strategy

In MoCET, the number of expert layers scales with the token count, as each new token requires an additional expert block. While this design yields strong reconstruction, it also increases training costs. To mitigate this, based on Titok's[37] two-stage training approach, we propose the **Hierarchical Native Training** strategy.

As shown in Fig. 3, we first train a 32-token NativeTok with full parameters. For the 64-token version, we reuse the Meta Image Transformer and the first 32 experts, duplicating their weights into the new experts. We then freeze the reused modules and train only the newly added 32 experts and a decoder, reducing trainable parameters to 56%. The same procedure applies to the 128-token model, where only the additional experts are trained. To further boost reconstruction quality, we freeze parameters for 90% of the steps and perform full fine-tuning in the last 10%.

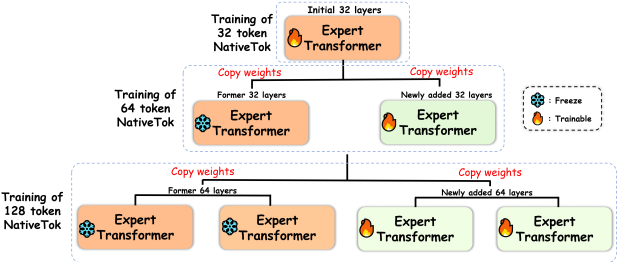


Figure 3 Hierarchical Native Training: We freeze the Meta Image Transformer and existing experts, training only newly added experts initialized with reused weights. This reduces training costs while ensuring the new experts inherit prior modeling capabilities.

4 Experiments

4.1 Experimental Setups

We evaluate our method on class-conditional ImageNet-1K[8] with 256×256 image resolution. The standard Fréchet Inception Distance (FID)[17] is adopted for evaluating the reconstruction and generation quality (denoted as rFID and gFID). rFID is calculated over the entire validation set. gFID follows ADM [9] by generating 50K samples for FID evaluation in the context of image generation.

4.2 Main Experiment

To evaluate the impact of *native visual tokenization* on generation quality, we conduct experiments under both autoregressive (AR) and MaskGIT-style paradigms. For AR generation, we compare NativeTok₃₂ against TiTok-L-32 [37] and VQGAN, using LlamaGen-B as the generator. As shown in Table 1, our method achieves a 0.23 improvement in gFID over VQGAN. When the final token sequence length is fixed at 32, NativeTok significantly outperforms TiTok-L-32 [37], reducing the gFID from 7.45 to 5.23. Notably, despite a slightly worse reconstruction metric (rFID = 2.57), NativeTok achieves better generation performance under the same AR generator.

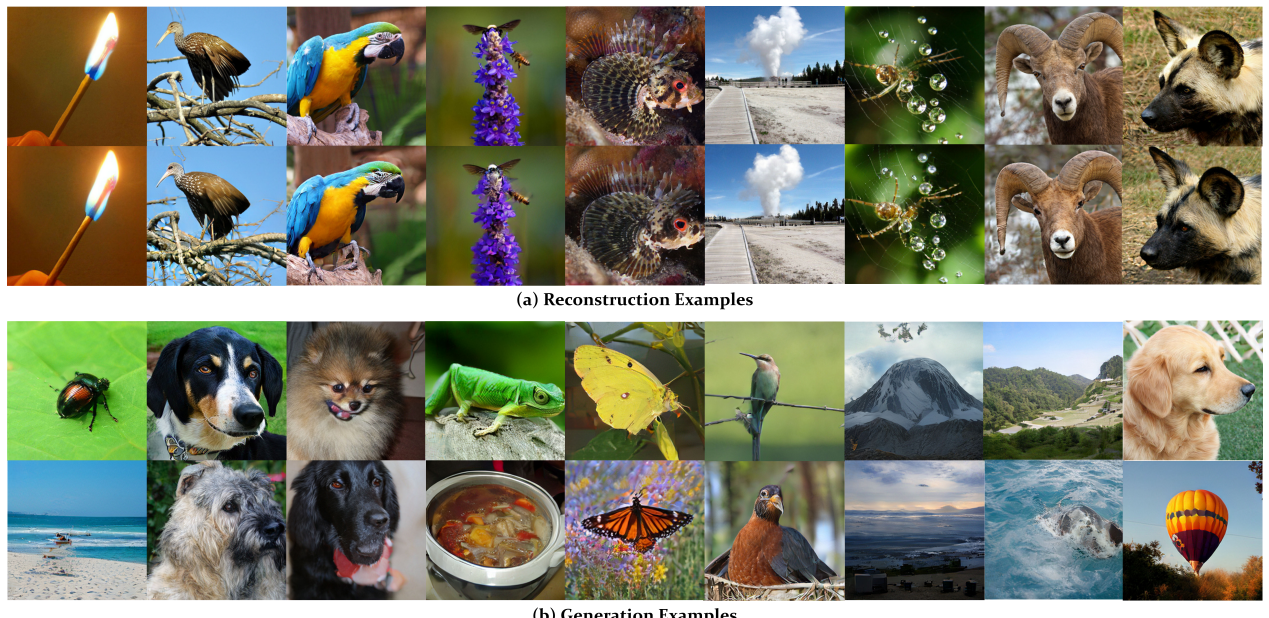


Figure 4 In (a), the top and bottom rows correspond to the original images and their reconstructed results. In (b), we showcase examples of generated images.

Tokenizer	#Params	#Tokens	rFID ↓	(LlamaGen-B) gFID ↓
VQGAN	72M	256	2.19	5.46
TiTok-L-32	641M	32	2.21	7.45
NativeTok ₃₂	616M	32	2.57	5.23

Table 1 Main comparison of AR generation performance. *Params* denotes the number of parameters in the tokenizer. *Tokens* denotes the length of the token sequence produced during the tokenization stage. All gFID scores are reported using LlamaGen-B as the generator.

In Table 2, we further compare the best-performing version of NativeTok, which is NativeTok₁₂₈ within the MaskGIT framework, using MaskGIT-UVit-L [2, 5] as the generator, with several state-of-the-art methods.

Under this generation paradigm, NativeTok achieves a gFID of 2.16 with only 287M params, demonstrating strong generation performance. This set of experiments confirms that the ordered token sequences generated

Tokenizer	#Tokens	Codebook Size	rFID \downarrow	Generator	gFID \downarrow	P \downarrow	Gen-Type
VAE	1024 \times 4	-	0.62	UViT-L/2 DiT-XL/2 SiT-XL/2	3.40	287M	Diffusion
					2.27	675M	Diffusion
					2.06	675M	Diffusion
<i>diffusion-based generative models</i>							
RQ-VAE MaskGIT-VQGAN ViT-VQGAN VQGAN GigaTok-S-S TiTok-S-128 VAR MAR-KL-16 MAGVIT-v2 FlexTok(d18-d18)	256	16384	3.20	RQ-Transformer	4.45	1.4B	AR
	256	1024	2.28	MaskGIT-ViT	7.55	3.8B	Mask
	1024	8192	1.28	VIM-Large	4.17	1.7B	AR
	256	16384	2.19	LlamaGen-B	5.46	111M	AR
				LlamaGen-L	4.21	343M	AR
				LlamaGen-B	4.05	111M	AR
	256	16384	1.01	MaskGIT-UViT-L	2.50	287M	Mask
	128	4096	1.71	MaskGIT-UViT-L	1.97	287M	Mask
	680	>4096	0.90	VAR transformer	1.92	2B	AR
	256	-	1.22	MAR-H	2.35	943M	AR
NativeTok ₁₂₈	256	16384	1.39	Open-MAGVIT2-AR-L	2.51	804M	AR
	256	64000	1.61	AR Transformers	2.02	1.33B	AR
<i>transformer-based generative models</i>							
<i>Ours</i>							
NativeTok ₁₂₈	128	4096	1.19	MaskGIT-UViT-L	2.16	287M	Mask

Table 2 Comparison of Tokenizers and Generators. In the table, **P** denotes the number of model parameters, and **Gen.Type** denotes the generative model type. Specifically, for TiTok-S-128, 2.50 and 1.97 represent the results of 8 and 64 sampling steps, respectively, while the 2.16 result for NativeTok₁₂₈ is obtained with 8 sampling steps.

by NativeTok consistently improve generation quality in both AR and MaskGIT-style settings. **Since the second-stage generative model essentially learns the distribution established during tokenization, introducing token-level constraints enables more structured and learnable dependencies.** Examples of reconstruction and generation results are presented in Fig. 4.

4.3 Ablations

Model	#Params	FID \downarrow	Model	Strategy	rFID \downarrow	Speed \downarrow	model	Sample/s
Titok _{L-32}	641M	12.99	NativeTok ₆₄	full	6.50	1.53s	VQGAN	233.02
Titok _{L(mask)-32}	641M	12.95	NativeTok ₆₄	reuse	6.46	1.15s	Titok-L-32	136.32
NativeTok ₃₂	616M	11.19	NativeTok ₆₄	reuse + fine tune	6.22	-	NativeTok ₃₂	119.85

(a) Different Attention Mechanisms.

(b) Training Strategies Comparison.

(c) Encoding Speed Comparison.

Comparison of different attention mechanisms: In Table 3a, we compare different attention mechanisms used in NativeTok. We first conducted a comparative analysis of Titok_{L-32}, Titok_{L(mask)-32} (which incorporates causal masks into its encoder), and NativeTok₃₂. This comparison further validates the structural efficiency of our proposed framework, especially when compared to traditional approaches that simply apply causal masks at the model input level, as the rFID significantly decreases from 12.99 and 12.95 to 11.19 under the same number of training steps.

Comparison of Different Training Strategies. Experiments here is designed to evaluate the efficiency of the proposed Hierarchical Native Training strategy and to identify the optimal training configuration which are conducted on two A800 GPUs with a per-GPU batch size of 64. In Table 3b, we conduct experiments on NativeTok₆₄ using three training strategies: (1) full-parameter training with random initialization, (2) full reuse of pretrained weights without modification (3) reuse training for 90% of the steps followed by full-parameter fine-tuning in the remaining 10%. Results show that the Hierarchical Native Training strategy significantly improves training efficiency, reducing time per batch from 1.53s to 1.15s. At the same time, rFID improves from 6.50 to 6.46. After an additional 10% of full-parameter fine-tuning, rFID is further reduced to 6.22, demonstrating the efficiency of this training strategy.

Comparison of Encoding Speed. As shown in Table 3c, although NativeTok employs a longer MoCET sequence, its attention modeling is performed in a low-dimensional latent space. Owing to the $\mathcal{O}(n^2)$ complexity of

transformers, this results in a moderate drop in encoding speed. However, the impact remains limited and does not significantly affect overall efficiency.

4.4 Visualization

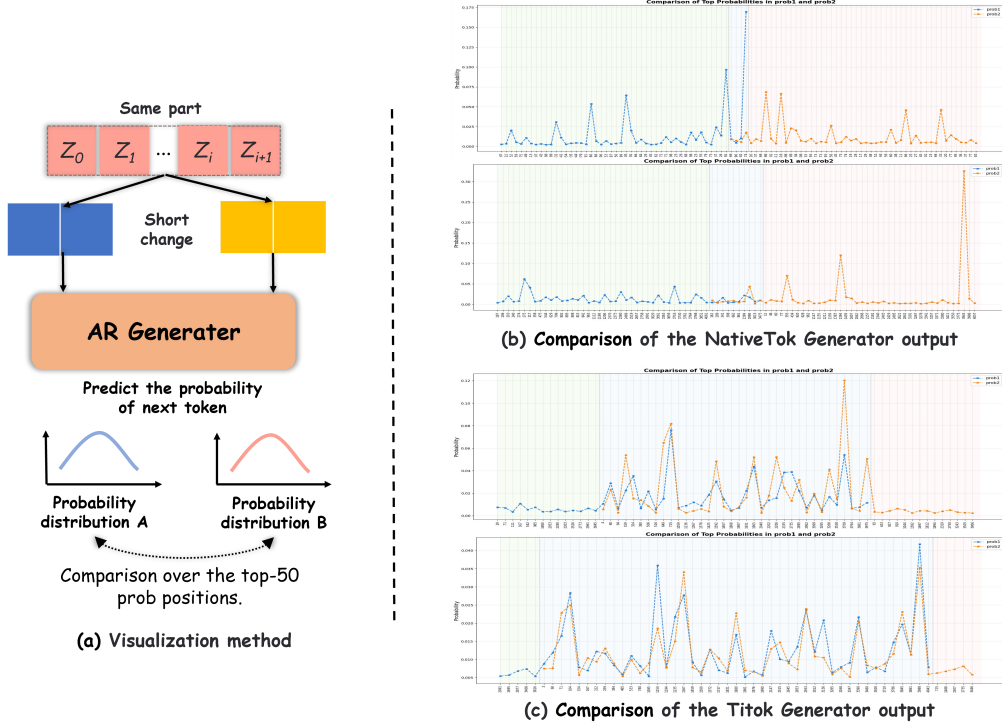


Figure 5 Visualization: In the right-hand figure, the x-axis denotes the token position index, and the y-axis represents the corresponding probability values. When modifying adjacent token representations, we compare how the probability distribution of the next token changes accordingly.

In Fig. 5, we present visualization results that highlight the accuracy of NativeTok’s token sequence to perturbations in preceding tokens. To investigate this, we first input a condition C into the generator and set two indices, i and j . Tokens before position i are deterministically selected as the most probable choices, while tokens between positions i and j are sampled according to their probability distribution. We then visualize the probability distribution of the token generated at position $j+1$. Specifically, we extract the top-100 highest-probability positions from the output distributions of the same generator under two slightly different inputs. We categorize these into overlapping and non-overlapping subsets for comparison. Fig. 5(b) and Fig. 5(c) show the results for $NativeTok_{32}$ and $TiTok_{L-32}$, respectively, under two settings: modifying 2 tokens (top row) and 4 tokens (bottom row). This observation is further supported by quantitative metrics showing a significant drop in the overlap of high-probability positions in the final token distribution, demonstrate that NativeTok yields a smaller overlapping region, suggesting that the generator models its token sequences with greater sensitivity and accuracy.

5 Conclusion

We propose the concept of *native visual tokenization* and introduce *NativeTok*, a novel visual tokenizer that encodes images into ordered token sequences aligned with generation stage. By incorporating a native visual order and hierarchical training strategy, NativeTok bridges the gap between tokenization and generation, enabling improved image generation.

6 Acknowledgment

This research is supported by National Natural Science Foundation of China under Grant 623B2094.

References

- [1] Roman Bachmann, Jesse Allardice, David Mizrahi, Enrico Fini, Oğuzhan Fatih Kar, Elmira Amirloo, Alaaeldin El-Nouby, Amir Zamir, and Afshin Dehghan. Flextok: Resampling images into 1d token sequences of flexible length. [arXiv preprint arXiv:2502.13967](#), 2025.
- [2] Fan Bao, Shen Nie, Kaiwen Xue, Yue Cao, Chongxuan Li, Hang Su, and Jun Zhu. All are worth words: A vit backbone for diffusion models. In [Proceedings of the IEEE/CVF conference on computer vision and pattern recognition](#), pages 22669–22679, 2023.
- [3] Kaj Bostrom and Greg Durrett. Byte pair encoding is suboptimal for language model pretraining. [arXiv preprint arXiv:2004.03720](#), 2020.
- [4] Shiyue Cao, Yueqin Yin, Lianghua Huang, Yu Liu, Xin Zhao, Deli Zhao, and Kaigi Huang. Efficient-vqgan: Towards high-resolution image generation with efficient vision transformers. In [Proceedings of the IEEE/CVF International Conference on Computer Vision](#), pages 7368–7377, 2023.
- [5] Huiwen Chang, Han Zhang, Lu Jiang, Ce Liu, and William T Freeman. Maskgit: Masked generative image transformer. In [Proceedings of the IEEE/CVF conference on computer vision and pattern recognition](#), pages 11315–11325, 2022.
- [6] Hao Chen, Ze Wang, Xiang Li, Ximeng Sun, Fangyi Chen, Jiang Liu, Jindong Wang, Bhiksha Raj, Zicheng Liu, and Emad Barsoum. Softvq-vae: Efficient 1-dimensional continuous tokenizer. [arXiv preprint arXiv:2412.10958](#), 2024.
- [7] Hao Chen, Yujin Han, Fangyi Chen, Xiang Li, Yidong Wang, Jindong Wang, Ze Wang, Zicheng Liu, Difan Zou, and Bhiksha Raj. Masked autoencoders are effective tokenizers for diffusion models. [arXiv preprint arXiv:2502.03444](#), 2025.
- [8] Jia Deng, Wei Dong, Richard Socher, Li-Jia Li, Kai Li, and Li Fei-Fei. Imagenet: A large-scale hierarchical image database. In [2009 IEEE conference on computer vision and pattern recognition](#), pages 248–255. Ieee, 2009.
- [9] Prafulla Dhariwal and Alexander Nichol. Diffusion models beat gans on image synthesis. [Advances in neural information processing systems](#), 34:8780–8794, 2021.
- [10] Ming Ding, Zhuoyi Yang, Wenyi Hong, Wendi Zheng, Chang Zhou, Da Yin, Junyang Lin, Xu Zou, Zhou Shao, Hongxia Yang, et al. Cogview: Mastering text-to-image generation via transformers. [Advances in neural information processing systems](#), 34:19822–19835, 2021.
- [11] Alexey Dosovitskiy, Lucas Beyer, Alexander Kolesnikov, Dirk Weissenborn, Xiaohua Zhai, Thomas Unterthiner, Mostafa Dehghani, Matthias Minderer, Georg Heigold, Sylvain Gelly, et al. An image is worth 16x16 words: Transformers for image recognition at scale. [arXiv preprint arXiv:2010.11929](#), 2020.
- [12] Patrick Esser, Robin Rombach, and Bjorn Ommer. Taming transformers for high-resolution image synthesis. In [Proceedings of the IEEE/CVF conference on computer vision and pattern recognition](#), pages 12873–12883, 2021.
- [13] Hongchang Gao, Jian Pei, and Heng Huang. Progan: Network embedding via proximity generative adversarial network. In [Proceedings of the 25th ACM SIGKDD International Conference on Knowledge Discovery & Data Mining](#), pages 1308–1316, 2019.
- [14] Shanghua Gao, Pan Zhou, Ming-Ming Cheng, and Shuicheng Yan. Masked diffusion transformer is a strong image synthesizer. In [Proceedings of the IEEE/CVF international conference on computer vision](#), pages 23164–23173, 2023.
- [15] Ian Goodfellow, Jean Pouget-Abadie, Mehdi Mirza, Bing Xu, David Warde-Farley, Sherjil Ozair, Aaron Courville, and Yoshua Bengio. Generative adversarial nets. [Advances in neural information processing systems](#), 27, 2014.
- [16] Shuyang Gu, Dong Chen, Jianmin Bao, Fang Wen, Bo Zhang, Dongdong Chen, Lu Yuan, and Baining Guo. Vector quantized diffusion model for text-to-image synthesis. In [Proceedings of the IEEE/CVF conference on computer vision and pattern recognition](#), pages 10696–10706, 2022.

[17] Martin Heusel, Hubert Ramsauer, Thomas Unterthiner, Bernhard Nessler, and Sepp Hochreiter. Gans trained by a two time-scale update rule converge to a local nash equilibrium. *Advances in neural information processing systems*, 30, 2017.

[18] Jonathan Ho, Ajay Jain, and Pieter Abbeel. Denoising diffusion probabilistic models. *Advances in neural information processing systems*, 33:6840–6851, 2020.

[19] Mengqi Huang, Zhendong Mao, Zhuowei Chen, and Yongdong Zhang. Towards accurate image coding: Improved autoregressive image generation with dynamic vector quantization. In *Proceedings of the IEEE/CVF Conference on Computer Vision and Pattern Recognition (CVPR)*, pages 22596–22605, June 2023.

[20] Tero Karras, Samuli Laine, and Timo Aila. A style-based generator architecture for generative adversarial networks. In *Proceedings of the IEEE/CVF conference on computer vision and pattern recognition*, pages 4401–4410, 2019.

[21] Tero Karras, Samuli Laine, Miika Aittala, Janne Hellsten, Jaakko Lehtinen, and Timo Aila. Analyzing and improving the image quality of stylegan. In *Proceedings of the IEEE/CVF conference on computer vision and pattern recognition*, pages 8110–8119, 2020.

[22] Doyup Lee, Chiheon Kim, Saehoon Kim, Minsu Cho, and Wook-Shin Han. Autoregressive image generation using residual quantization. In *Proceedings of the IEEE/CVF Conference on Computer Vision and Pattern Recognition*, pages 11523–11532, 2022.

[23] Tianhong Li, Huiwen Chang, Shlok Mishra, Han Zhang, Dina Katabi, and Dilip Krishnan. Mage: Masked generative encoder to unify representation learning and image synthesis. In *Proceedings of the IEEE/CVF Conference on Computer Vision and Pattern Recognition*, pages 2142–2152, 2023.

[24] Fabian Mentzer, David Minnen, Eirikur Agustsson, and Michael Tschannen. Finite scalar quantization: Vq-vae made simple. *arXiv preprint arXiv:2309.15505*, 2023.

[25] William Peebles and Saining Xie. Scalable diffusion models with transformers. In *Proceedings of the IEEE/CVF international conference on computer vision*, pages 4195–4205, 2023.

[26] Dustin Podell, Zion English, Kyle Lacey, Andreas Blattmann, Tim Dockhorn, Jonas Müller, Joe Penna, and Robin Rombach. Sdxl: Improving latent diffusion models for high-resolution image synthesis. *arXiv preprint arXiv:2307.01952*, 2023.

[27] Ali Razavi, Aaron Van den Oord, and Oriol Vinyals. Generating diverse high-fidelity images with vq-vae-2. *Advances in neural information processing systems*, 32, 2019.

[28] Robin Rombach, Andreas Blattmann, Dominik Lorenz, Patrick Esser, and Björn Ommer. High-resolution image synthesis with latent diffusion models. In *Proceedings of the IEEE/CVF conference on computer vision and pattern recognition*, pages 10684–10695, 2022.

[29] Yusuke Shibata, Takuya Kida, Shuichi Fukamachi, Masayuki Takeda, Ayumi Shinohara, Takeshi Shinohara, and Setsuo Arikawa. Byte pair encoding: A text compression scheme that accelerates pattern matching. 1999.

[30] Peize Sun, Yi Jiang, Shoufa Chen, Shilong Zhang, Bingyue Peng, Ping Luo, and Zehuan Yuan. Autoregressive model beats diffusion: Llama for scalable image generation. *arXiv preprint arXiv:2406.06525*, 2024.

[31] Keyu Tian, Yi Jiang, Zehuan Yuan, Bingyue Peng, and Liwei Wang. Visual autoregressive modeling: Scalable image generation via next-scale prediction. *Advances in neural information processing systems*, 37:84839–84865, 2025.

[32] Aaron Van Den Oord, Oriol Vinyals, et al. Neural discrete representation learning. *Advances in neural information processing systems*, 30, 2017.

[33] Ashish Vaswani, Noam Shazeer, Niki Parmar, Jakob Uszkoreit, Llion Jones, Aidan N Gomez, Łukasz Kaiser, and Illia Polosukhin. Attention is all you need. *Advances in neural information processing systems*, 30, 2017.

[34] Tianwei Xiong, Jun Hao Liew, Zilong Huang, Jiashi Feng, and Xihui Liu. Gigatok: Scaling visual tokenizers to 3 billion parameters for autoregressive image generation. *arXiv preprint arXiv:2504.08736*, 2025.

[35] Jiahui Yu, Xin Li, Jing Yu Koh, Han Zhang, Ruoming Pang, James Qin, Alexander Ku, Yuanzhong Xu, Jason Baldridge, and Yonghui Wu. Vector-quantized image modeling with improved vqgan. *arXiv preprint arXiv:2110.04627*, 2021.

- [36] Jiahui Yu, Yuanzhong Xu, Jing Yu Koh, Thang Luong, Gunjan Baid, Zirui Wang, Vijay Vasudevan, Alexander Ku, Yinfei Yang, Burcu Karagol Ayan, et al. Scaling autoregressive models for content-rich text-to-image generation. *arXiv preprint arXiv:2206.10789*, 2(3):5, 2022.
- [37] Qihang Yu, Mark Weber, Xueqing Deng, Xiaohui Shen, Daniel Cremers, and Liang-Chieh Chen. An image is worth 32 tokens for reconstruction and generation. *Advances in Neural Information Processing Systems*, 37: 128940–128966, 2025.
- [38] Chuanxia Zheng, Tung-Long Vuong, Jianfei Cai, and Dinh Phung. Movq: Modulating quantized vectors for high-fidelity image generation. *Advances in Neural Information Processing Systems*, 35:23412–23425, 2022.

NativeTok: Native Visual Tokenization for Improved Image Generation

Appendix

F.1 Training and Testing Protocols

Configuration	Value
<i>NativeTok₃₂</i>	
Meta Image Transformer layers	18
Meta Image Transformer dim	1024
MoCET layers	32
MoCET dim	256
decoder layers	24
decoder dim	1024
total parameters	616M
training strategy	full param training
Trainable params rate	100%
speed	63.44/s/gpu Batch
<i>NativeTok₆₄</i>	
Meta Image Transformer layers	18
Meta Image Transformer dim	1024
MoCET layers	64
MoCET dim	256
decoder layers	24
decoder dim	1024
total parameters	666M
training strategy	HNT strategy
Trainable params rate	56%
speed	54.14/s/gpu Batch
speed of full parameter fine-tune	40.48/s/gpu Batch
<i>NativeTok₁₂₈</i>	
Meta Image Transformer layers	18
Meta Image Transformer dim	1024
MoCET layers	128
MoCET dim	256
decoder layers	24
decoder dim	1024
total parameters	766M
training strategy	HNT strategy
Trainable params rate	55%
speed	39.44/s/gpu Batch
speed of full parameter fine-tune	30.75/s/gpu Batch
<i>Training Configuration</i>	
dataset	ImageNet1K
image resolution	256×256
random crop	True
random flip	True
device	NVIDIA A800 × 4
per gpu batch size	64
global batch size	256
optimizer	AdamW
base learning rate	1e ⁻⁴
learning rate schedule	cosine
end learning rate	1e ⁻⁵
warmup steps	5K
weight decay	1e ⁻⁴
optimizer momentum	$\beta_1, \beta_2 = 0.9, 0.99$
training steps	500K

Table 4 Configuration of NativeTok.

For image generation using **NativeTok**, we provide the configuration and training strategies across three model scales: *NativeTok*₃₂, *NativeTok*₆₄, and *NativeTok*₁₂₈. All models are trained on ImageNet-1K at resolution 256×256 with center cropping and horizontal flipping as the only augmentations.

For NativeTok₃₂, we use a Meta Image Transformer with 18 layers and 1024 hidden dimensions, followed by a Mixture of Causal Expert Transformer composed of 32 layers with 256 hidden dimensions. The decoder has 24 layers and 1024 hidden dimensions. This model contains a total of 616M parameters and is trained with full parameter updates. The training throughput is 63.44 samples per second per GPU.

For NativeTok₆₄, we increase the Mixture of Causal Expert Transformer to 64 layers while keeping other components unchanged. The model size grows to 666M parameters. We employ the Hierarchical Native Training (HNT) strategy over 450K training steps, resulting in only 56% of parameters being updated during initial training. The training speed is 54.14 samples/s/GPU, and 40.48 samples/s/GPU for full-parameter fine-tuning.

For NativeTok₁₂₈, we maintain the same architecture as *NativeTok*₆₄ but scale the training to a larger Mixture of Experts model with the same 64 expert layers. The parameter count rises to 766M. HNT strategy is used again with 55% trainable parameters. Training throughput is 39.44 samples/s/GPU, dropping to 30.75 samples/s/GPU for full fine-tuning.

Training configuration. All models are trained using 4 NVIDIA A800 GPUs with a per-GPU batch size of 64 (global batch size 256). We use the AdamW optimizer with $\beta_1 = 0.9$, $\beta_2 = 0.99$, a base learning rate of 1×10^{-4} , cosine decay schedule down to 1×10^{-5} , and weight decay of 1×10^{-4} . The warm-up phase lasts 5K steps, and the full training takes 500K steps.

Hierarchical Native Training strategy. For larger model variants (*NativeTok*₆₄ and *NativeTok*₁₂₈), we use the Hierarchical Native Training (HNT) strategy, which gradually expands trainable parameter subsets to mitigate optimization difficulty in large-scale mixtures of experts.

We provide the complete configuration in table 4.

F.2 Detailed Results of Preliminary Experiments

Model	Params \downarrow	rFID \downarrow
stage1		
NativeTok ₃₂	616M	5.10
NativeTok ₆₄	666M	3.54
NativeTok ₁₂₈	766M	2.86
add decoder finetune		
NativeTok ₃₂	616M	2.57
NativeTok ₆₄	666M	1.89
NativeTok ₁₂₈	766M	1.19

Table 5 Detailed Performance of NativeTok.

Detailed Performance of NativeTok. We report the performance of different NativeTok variants across both training stages, as summarized in Table 5.

To quantitatively assess reconstruction quality, we measure rFID scores (lower is better) under two settings: *Stage 1 only* and *Stage 1 + decoder fine-tuning*. As shown in Table 5, increasing model capacity from NativeTok₃₂ to NativeTok₁₂₈ consistently enhances reconstruction quality. Under Stage 1 alone, the rFID decreases from 5.10 to 2.86 with increasing model scale. With additional decoder fine-tuning, the rFID further improves to 2.57, 1.89, and 1.19 for NativeTok₃₂, NativeTok₆₄, and NativeTok₁₂₈, respectively.

In addition, the parameter count reflects the impact of increasing the number of experts in the MoCET module. Although larger token counts result in more MoCET parameters, the increase is sublinear: every additional 32 tokens introduce only about an 8% increase in parameters relative to the base model.

F.3 Qualitative Visualization

We provide more detailed quantitative metrics corresponding to the visualization section in the main paper in Table 6. Specifically, we modify short token subsequences of varying lengths from 1 to 4 and compute the average top-100 overlap rate across 1,000 ImageNet classes. We compare the results of NativeTok and TiTok under the same setting. The results show that NativeTok consistently exhibits a lower overlap rate, indicating that the generator is more sensitive to token-level variations. This reflects a stronger alignment between the token representations and the generation behavior, resulting in more precise outputs.

We provide several reconstruction visualizations in Figure 7. From left to right: original image, NativeTok₁₂₈ reconstruction, NativeTok₆₄ reconstruction, and NativeTok₃₂ reconstruction.

Number of Inconsistent Tokens	NativeTok Overlap Ratio	TiTok Overlap Ratio
1	56.26%	78.66%
2	50.89%	75.78%
3	48.34%	73.43%
4	48.44%	68.37%

Table 6 Comparison of Token Overlap Ratios between NativeTok and TiTok.

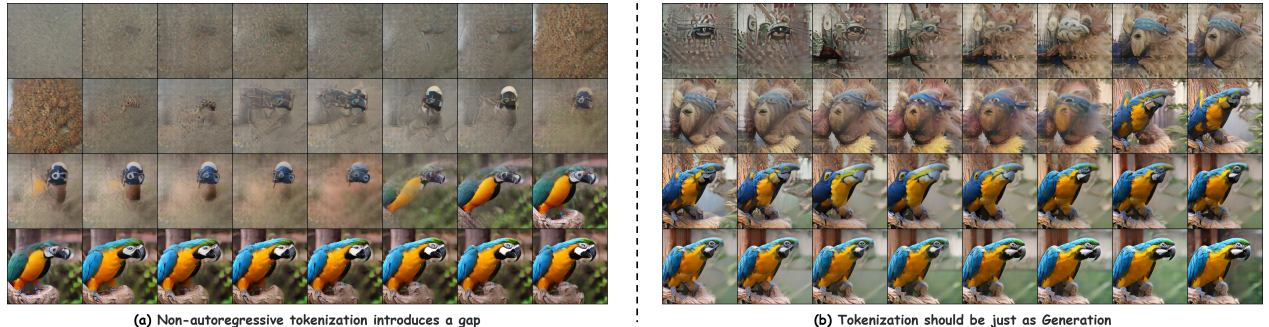


Figure 6 Reconstructions during the token generation process where the token count increases from 0 to 32.

In Figure 6, we visualize the morphological changes of NativeTok₃₂ and Titok₃₂ reconstructions during the token generation process where the token count increases from 0 to 32. Our observations reveal that: Under Titok₃₂’s bidirectional attention mechanism, earlier tokens inherently contain information from subsequent tokens. In contrast, NativeTok₃₂ with unidirectional attention progressively incorporates novel visual information not present in previous tokens.

We provide several qualitative examples of generated images in Figure 8.

F.4 Limitations

While our proposed method demonstrates promising performance in both reconstruction and generation tasks, several limitations remain to be addressed in future work.

Two-stage Training Pipeline. Similar to previous methods such as TiTok, our framework still adopts a two-stage training scheme, where the image tokenizer is trained independently from the autoregressive generative model. Although we partially alleviate the gap between these stages through hierarchical causal training and

decoder fine-tuning, a fully unified end-to-end training pipeline remains unexplored. Bridging this gap could further improve token quality and model coherence, especially in downstream autoregressive tasks.

Limited Training Scale. Due to computational constraints and limited resources, we were only able to train the autoregressive generator using the smallest variant, *NativeTok32*. While this variant already shows clear advantages over its TiTok counterpart, it does not fully exploit the benefits of higher-capacity tokenizers like *NativeTok128*. As a result, our generation results may not reflect the upper bound of our proposed framework’s potential. Future work will include large-scale training of the autoregressive model on more capable tokenizer variants, which is expected to yield further improvements.

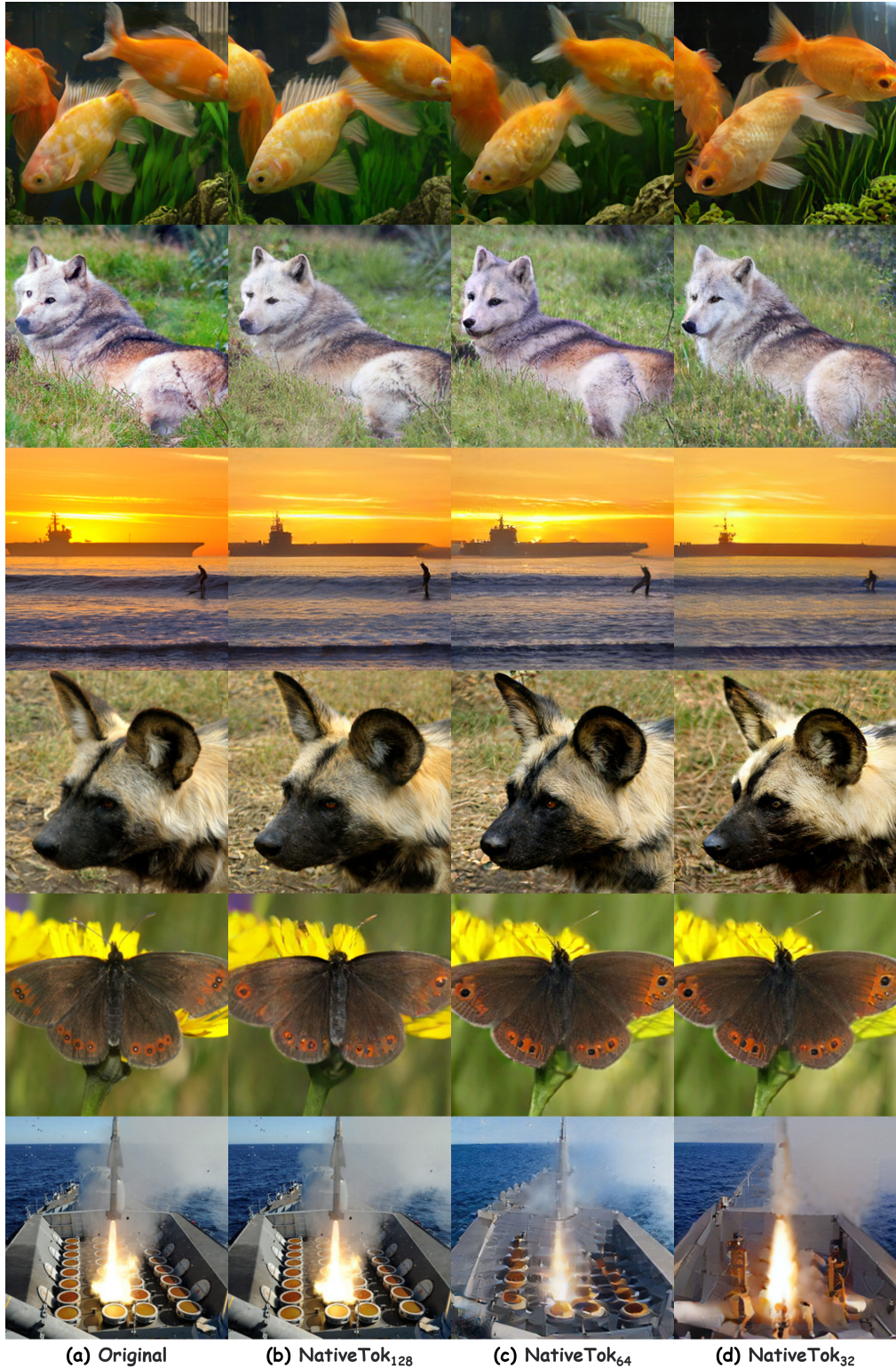
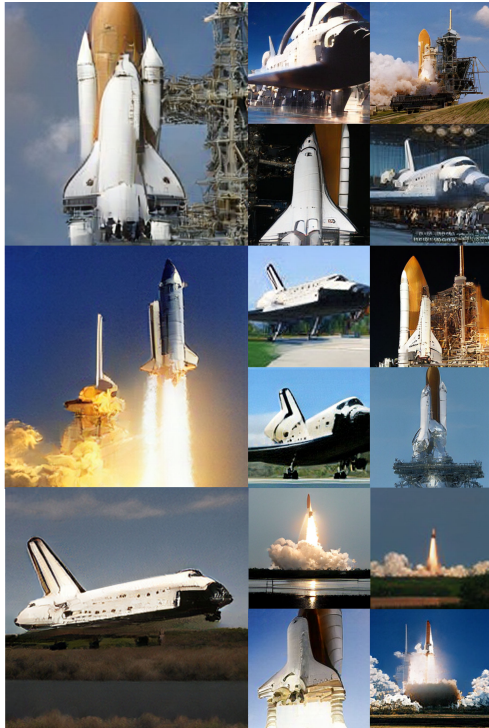


Figure 7 We provide a demonstration of reconstruction results. From left to right: the original image, reconstruction image by NativeTok₁₂₈, reconstruction image by NativeTok₆₄, and reconstruction image by NativeTok₃₂.



(a) Space shuttle: 812



(b) Monarch butterfly: 323



(c) Golden retriever: 207



(d) Hot air balloon: 417

Figure 8 Generation examples